EAI Endorsed Transactions
on Scalable Information Systems
Research Article EAI.EU

Image Quality Assessment of Multi-Satellite Pan-Sharpening Approach: A Case Study using Sentinel-2 Synthetic Panchromatic Image and Landsat-8

Greetta Pinheiro[1*], Ishfaq Hussain Rather[1], Aditya Raj[1], Sonajharia Minz[1], Sushil Kumar[1]

[1]Jawaharlal Nehru University, New Delhi, 110067, India

Abstract

INTRODUCTION: The satellite's physical and technical capabilities limit high spectral and spatial resolution image acquisition. In Remote Sensing (RS), when high spatial and spectral resolution data is essential for specific Geographic Information System (GIS) applications, Pan Sharpening (PanS) becomes imperative in obtaining such data.
OBJECTIVES: Study aims to enhance the spatial resolution of the multispectral Landsat-8 (L8) images using a synthetic panchromatic band generated by averaging four fine-resolution bands in the Sentinel-2 (S2) images.
METHODS: Evaluation of the proposed multi-satellite PanS approach, three different PanS techniques, Smoothed Filter Intensity Modulation (SFIM), Gram-Schmidt (GS), and High Pass Filter Additive (HPFA) are used for two different study areas. The techniques' effectiveness was evaluated using well-known Image Quality Assessment Metrics (IQAM) such as Root Mean Square Error (RMSE), Correlation Coefficient (CC), Erreur Relative Globale Adimensionnelle de Synthèse (ERGAS), and Relative Average Spectral Error (RASE). This study leveraged the GEE platform for datasets and implementation.
RESULTS: The promising values were provided by the GS technique, followed by the SFIM technique, whereas the HPFA technique produced the lowest quantitative result.
CONCLUSION: In this study, the spectral bands of the MS image's performance show apparent variation with respect to that of the different PanS techniques used.

Keywords: Pan-sharpening, Multispectral images, Panchromatic image, Landsat-8, Sentinel-2, Remote Sensing, Image Quality Assessment Metrics

Received on 16 December 2023, accepted on 14 March 2024, published on 21 March 2024

doi: 10.4108/eetsis.5496

*Corresponding author. Email: greett17_scs@jnu.ac.in

1 Introduction

In remote sensing, composing images from multiple sources to create a single image by harnessing the best characteristics of all the sources is called image fusion [1]–[5]. The image fusion, which merges the spatial information from the Panchromatic (PAN) band with higher resolution with the multispectral (MS) bands with lower resolution for obtaining a higher resolution MS image, is termed Pan Sharpening (PanS) [6]–[8].
The PanS draws much research interest because the technical and financial constraints limit the direct acquisition of images with higher spatial and spectral resolution from all imaging systems. There are three categories of PanS techniques: feature-level, decision-level, and pixel-level [1], [9], [10]. At the decision level, the input images are processed separately to extract the decisions. These decisions are combined instead of the actual images [11]. The structural, geometrical, and spectral features like textures, edges, angles, and shapes are fused in feature-level PanS. The input image values are combined pixel-by-pixel in pixel-level PanS.
The pixel-level PanS techniques are the most frequently used PanS approach in remote sensing for generating high spatial and spectral fused images. The high frequency information extracted from the PAN image is injected on the resampled MS bands using various PanS models [12]. PanS methods enhance visual interpretation, improve image quality, and increase classification accuracy[13]. The reliability and accuracy obtained from the pan-sharpened image play a

crucial role in determining the quality of the successive image processing and analysis tasks using the input as the pan-sharpened image. The generated synthesized image quality relies mainly on the performances of the fusion algorithms used for the PanS process.

The fusion quality assessment of various PanS techniques is examined by various researchers [2], [3], [11]. However, selecting an optimal PanS technique is challenging. The effectiveness of various PanS techniques using different fusion quality assessment methods has been evaluated [3], [4], [11], [14]–[19]. Small datasets [20] are used for comparing the performance of newly introduced fusion algorithms with the existing benchmark methods [21], [22] and for comparing the performance of the current methods [3], [4], [6], [18]. In light of the different advantages and limitations associated with PanS techniques, fused image quality assessment is required before applying these techniques to different applications [23]. Moreover, visually evaluating the satellite images is essential, considering factors like patterns, scale, tones, colour, contrast, and shadows, which play a crucial role in interpreting the image [1].

Earth observation satellites, like Landsat, capture PAN bands with high-resolution (15m) and MS bands with lower resolution (30m) [24], [25]. Therefore, the PanS of PAN and MS bands becomes essential for generating MS image representation with higher resolution (15m). S2, on the other hand, has 13 bands but has no dedicated PAN with high resolution, while the spatial resolutions vary across bands ranging between 10m to 60m [26].

The 10m bands of S2 effectively captures the spatial details of the ground features, which are important while performing the image sharpening process. For generating synthetic PAN band, the major task is to fuse the coarse S2 bands (20m/60m) using the 10m fine resolution S2 bands [27]. However, researchers have created a synthetic PAN (synPAN) band using the four bands with fine spectral resolution and used it for S2 PanS [28]. Various studies have proposed different synPAN generation methods for S2 PanS. MS bands with high spatial resolution were used by [27] as synthetic bands. Averaging of all four fine-resolution bands for generating PAN was suggested by [28]. [29] in their study, the NIR band was selected as the PAN band for increasing the spatial resolution of a few bands. [26] reviewed the various S2 PanS methods and observed that all the PAN generation techniques give accurate results in downscaling 20 m bands.

To overcome the challenge of analyzing the remote sensing big data, Google Earth Engine (GEE) was developed by Google as a free cloud computing platform that consists of a wide array of datasets including pre-processed as well as raw data[30]. The coverage offered by GEE spans regional to global scales. The L8 archive in GEE includes imagery from 2013 to present and that of S2 is available from 2015 to present. Google's computing infrastructure is used by GEE for rapid analysis [31]. The time and effort required for various satellite preprocessing steps are considerably reduced by using GEE within its environment[32]. This can be utilized in numerous applications including multi-temporal, spatio-temporal, spatio-spectral applications such as inundation mapping [33], image fusion[19], PanS[18], land cover classification [34], [35], forest cover mapping[12] etc.

This paper proposes a multi-satellite PanS, where images from two different satellites are used, namely L8 and S2 satellites; one for obtaining the MS image and the other for generating the SynPAN image for PanS. A SynPAN image is generated by making use of a few bands from the S2 satellite, and the L8 OLI optical satellite image is pan-sharpened using different PanS techniques to obtain a resultant high-resolution pan-sharpened MS image. The resulting L8 fused image using multi-satellite PanS had an increased spatial resolution. The most popular PanS techniques were selected, such as SFIM, GS, and HPFA. The quantitative comparison of the methods involved using metrics such as RMSE, CC, RASE, and ERGAS. This study leveraged the GEE platform for datasets and the methods were implemented as separate Java scripts in GEE.

The main contributions of this study are summarized as:

- Firstly, a multi-satellite PanS model for pan-sharpening the MS bands (30m) of the L8 satellite is proposed. The model utilizes the generated SynPAN band (10m) from the S2 satellite.
- Secondly, PanS uses three different techniques namely HPFA, GS, and SFIM.
- Thirdly, we Assess the pan-sharpened results using IQAM namely RMSE, CC, ERGAS, and RASE.
- Lastly, the Implementation of the multi-satellite PanS model as a script in Google Earth Engine (GEE) is performed.

We organize the remaining portion of the paper as follows: In section 2, we provide an overview of the materials incorporated in this study. In section 3, we present the methods in detail. In section 4, we discuss evaluation methods and the outcomes of experiments. Finally, in section V, we provide the paper's conclusion.

2. Materials

Two study areas were selected for this research, marked as area-1 and area-2, from San Francisco, located on the Pacific coast and one of the biggest cities in the United States and in the state of California [18]. Renowned for its captivating tourist spots, pleasant weather, beaches, facilities, landmarks, distinctive cuisine, and diverse, multicultural community. San Francisco is known for its cultural, business, financial, and commercial center with a rich historical and traditional background. The 'Presidio of San Francisco' is selected as the study area-1, which lies on the northern tip of the San Francisco Peninsula, and area-2 is Golden Gate Park, which lies between the Richmond and Sunset districts of San Francisco. Figure 1. illustrates the city area with coordinates 37° 46' 26.2992" N and 122° 25' 52.6692" W of San Francisco, and the area-1 and area-2 are marked.

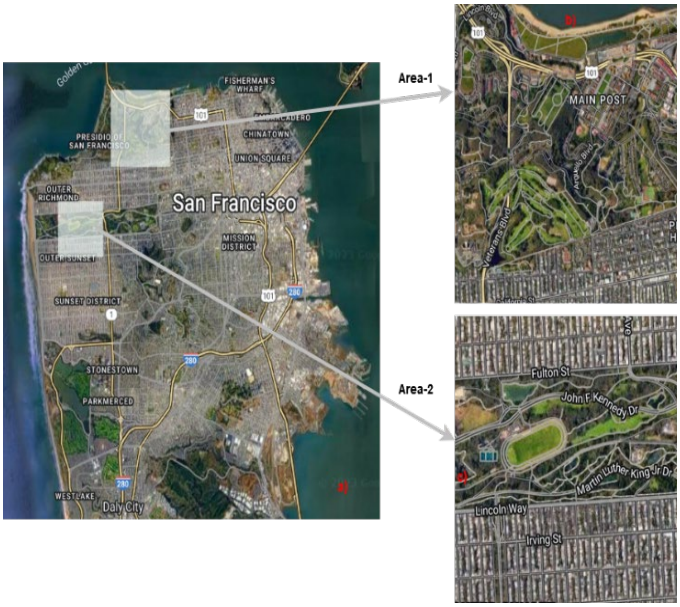

Figure 1. Study Area-1 and Area-2: San Francisco

The L8 OLI/TIRS combined satellite sensor image acquired on the 17th of April 2019, path 44, and row 34 were utilized for the study. Three bands of L8, namely band 2 (Blue), band 3 (Green), and band 4 (Red), each with 12-bit radiometric resolution, were employed as the lower-resolution MS image [36].

The MS imagery, depicted in Figures 3. a) and 3. b), has a 30 m spatial resolution. The S2 image was acquired on the 15th of April 2019; the band 2 (Blue), band 3 (Green), band 4 (Red), and band 8 (Visible and Near Infrared (VNIR)) have a spatial resolution of 10m. The RGB composite of S2 is as illustrated in Figures 3. c) and 3. d). The generated synPAN image has a 10 m spatial resolution and a radiometric resolution of 12-bit, as illustrated in Figures 3. g) and 3. h).

Experiments on the multi-satellite PanS help to assess the proposed S2 synPAN generation method's effectiveness and the resulting multi-satellite pan-sharpened image quality. All the applications in this research were performed using the Google Earth Engine. Area-1, covering the Presidio of San Francisco area in San Francisco, as shown in Figure 1 b) and Area-2, representing the Golden Gate Park, San Francisco, as depicted in Figure 1 c), consisted of images obtained from L8 and S2, with acquisition dates in Table 1.

Table 1. S2 and L8 acquisition dates for the study areas

	Data	Acquisition date
Landsat-8	LANDSAT/LC08/C01/T1_SR/ LC08_044034_20190417	17-04-2019
Sentinel-2	COPERNICUS/S2/20190415 T184919_20190415T190044 _T10SEG	15-04-2019

3. Methods

For enhancing the L8 satellite's spatial resolution for the RGB bands, a synPAN image was generated using four bands selected from the S2 satellite, namely bands 2, 3, 4, and 8, then averaging those fine-resolution bands. The research outlining this approach is explained in [28]. This study uses the generated S2 synPAN for multi-satellite PanS of the L8 MS satellite image's RGB bands. Figure 2. gives a detailed workflow of the proposed work. The PanS techniques used are outlined in this section.

Before performing the PanS techniques, it is important that the varying spatial resolutions of both synPAN and MS images need to be expressed at a similar spatial resolution. The upsampling of the MS image resolution to that of the synPAN image resolution is required and done using interpolation methods such as near or cubic. The PanS methods used in this research are introduced concisely. The data used in this study comprised corrected surface reflection products freely available from the Google Earth Engine data catalogue.

3.1 PanS Algorithms

This research uses three PanS techniques: HPFA, GS, and SFIM.

HPFA. The HPFA fusion process incorporates high-frequency information generated using the high-pass filter, which is applied to the SynPAN image while aiming to maintain the spectral features of the low-resolution image. It is an image fusion technique that falls under the spatial domain, integrating an image's high-resolution (HR) textural and structural attributes with a lower-resolution (LR) image. Compared to more complex PanS methods, HPFA achieves fusion by relying on simple square box high-pass filters, unlike wavelet-based techniques [37].

GS. The GS technique improves the MS image's spatial resolution while preserving its spectral characteristics. This technique creates a simulated SynPAN band by calculating the MS image's weighted sum of multiple bands, thus emulating the lowest spatial resolution among the MS bands. The determination of these weights considers the sensor's optical diffusion and spectral ranges of both the SynPAN and MS bands [3], [18].

Subsequently, the simulated SynPAN band is used as the initial band in the GS transformation. The GS technique is applied to the simulated SynPAN and MS bands. The statistics of the high pixel-sized SynPAN band are adjusted to ensure statistical balance in the first band of the GS transformations. With higher spatial resolution, this modified SynPAN band is then substituted for the first band of the GS transformation [38]. Finally, the MS image is generated

through inverse GS transforms, utilizing the spatial resolution of the SynPAN image.

SFIM is a technique that preserves the contrasts and spectral properties while effectively combining the spatial details of high-resolution (HR) SynPAN images with a co-registered low-resolution (LR) MS image. This modulation is achieved using the ratio between the HR SynPAN image and its corresponding low-pass filtered image, obtained through a smoothing filter [39].

3.2 Image Quality Evaluation of PanS Techniques

In PanS techniques, the MS image is resampled to the SynPAN images' spatial resolution. The spectral distortion can be evaluated using the source MS image with the dimensions corresponding to the SynPAN image [40].
RMSE utilizes statistical summaries such as mean, standard deviation, etc., coupled with the pixel values of the entire

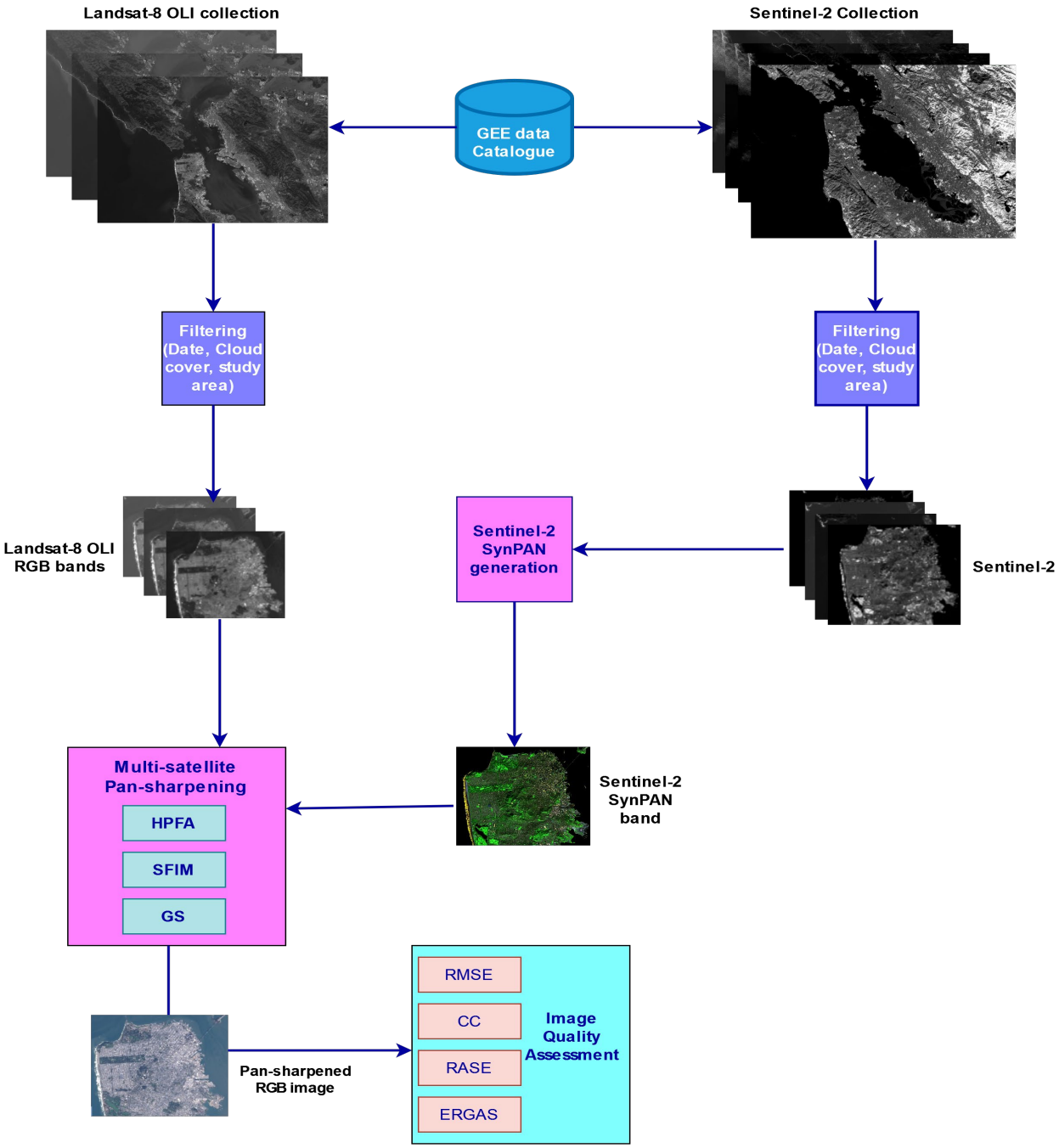

Figure 2: The flowchart representing the methodology used in this study

image are considered while computing the straightforward RMSE metrics calculations. Ps and R are the Pan-sharpened and reference images, respectively. The N denotes the total number of pixels. The RMSE metric computes the pan-sharpened image's level of correctness. As the squaring of the errors before calculating the average is performed, high weights are assigned for large errors in RMSE metrics. Therefore, RMSE is helpful in instances where the goal is avoiding large errors.

$$RMSE = \sqrt{\frac{\sum_{i=1}^{N}(F_i - R_i)^2}{N}} \quad (1)$$

CC calculations are performed between the reference and pan-sharpened image, representing the spectral characteristics' comparability [41]. The mean value of image R is represented as ($\bar{R}$) and that of the pan-sharpened image is represented as($\bar{P}s$). A spectral performance value equal to 1 is considered ideal for the pan-sharpened image.

$$\mathrm{CC}\left(\frac{R}{Ps}\right) = \frac{\sum_{i=1}^{N}(R_i - \bar{R})(Ps_i - \bar{P}s)}{\sqrt{\sum_{i=1}^{N}(R_i - \bar{R})^2 \sum_{i=1}^{N}(Ps_i - \bar{P}s)^2}} \quad (2)$$

RASE is deducted from RMSE; its effectiveness improves with respect to the decrease in the numerical value. Here, L indicates spectral bands, the mean radiance (μ), and B_i represents the i^{th} band of R.

$$\mathrm{RASE} = \frac{100}{\mu}\sqrt{\frac{1}{L}\sum_{i=1}^{L}\mathrm{RMSE}^2(B_i)} \quad (3)$$

ERGAS metric considers the ratios of the MS bands and the SynPAN band's spatial resolutions. The (h) indicates the MS image having higher spatial resolution, and (l) for the lower spatial resolution MS image.

$$\mathrm{ERGAS} = 100\frac{h}{l}\sqrt{\frac{1}{L}\sum_{i=1}^{L}\frac{\mathrm{RMSE}^2(B_i)}{\mu_i^2}} \quad (4)$$

4. Results and Discussion

The visual comparison alone would be insufficient in assessing the PanS; therefore, the quantitative assessment is considered in this work to evaluate the performances of techniques applied to the outcomes of various image fusion techniques and compare them. Following a visual assessment, the pan-sharpened images should be assessed statistically using image quality assessment metrics. Since the squaring of the errors before calculating the average is performed, RMSE assigns large errors with a higher weight. Therefore, RMSE is helpful in instances where evading large errors is required. The effectiveness of using RASE metrics increases with the decrease in numerical value as the RASE is deduced from RMSE. The ERGAS metric considers the MS bands and SynPAN band spatial resolution ratios along with the RMSE metric. The CC value nearer to 1 is regarded as the best.

A comparative assessment of the three PanS techniques for Area 1 is shown in Table 2 and Table 4, which for Area 2 are illustrated in Table 3, and Table 5.

Table 2. IQAM for HPFA, SFIM, and GS PanS techniques for multi-satellite pan-sharpened images for area-1

IQAM	HPFA	SFIM	GS
RASE	12.7688	9.0899	10.1492
ERGAS	1.8542	1.4926	1.4890

Table 3. IQAM for HPFA, SFIM, and GS PanS techniques for multi-satellite pan-sharpened images for area-2

IQAM	HPFA	SFIM	GS
RASE	12.7258	9.1199	10.1662
ERGAS	1.8472	1.4996	1.4908

Table 4. IQAM for HPFA, SFIM, and GS PanS techniques for multi-satellite pan-sharpened images corresponding to R, G, and B bands of L8 and the bands average for area-1.

IQAM	Band	HPFA	SFIM	GS
RMSE	Blue	0.0097	0.0064	0.0089
	Green	0.0102	0.0066	0.0073
	Red	0.0102	0.0075	0.0069
	Avg	0.0100	0.0068	0.0077
PCC	Blue	0.9789	0.9941	0.9878
	Green	0.9523	0.9808	0.9759
	Red	0.9699	0.9848	0.9935
	Avg	0.9670	0.9865	0.9857

Table 5. IQAM for HPFA, SFIM, and GS PanS techniques for multi-satellite pan-sharpened images corresponding to R, G, and B bands of L8 and the bands average for area-2.

IQAM	Band	HPFA	SFIM	GS
RMSE	Blue	0.0097	0.0090	0.0092
	Green	0.0101	0.0081	0.0085
	Red	0.0099	0.0078	0.0071
	Avg	0.0099	0.0083	0.0082
PCC	Blue	0.9696	0.9752	0.9768
	Green	0.9633	0.9900	0.9723
	Red	0.9599	0.9798	0.9864
	Avg	0.9642	0.9816	0.9785

The promising values were provided by the GS technique, followed by the SFIM technique, whereas the HPFA technique produced the lowest quantitative result. In this study, the spectral bands of the MS image's performance show apparent variation with respect to that of the different PanS techniques used.

Area-1

L8 (RGB) (30m)

S2 (RGB) (10m)

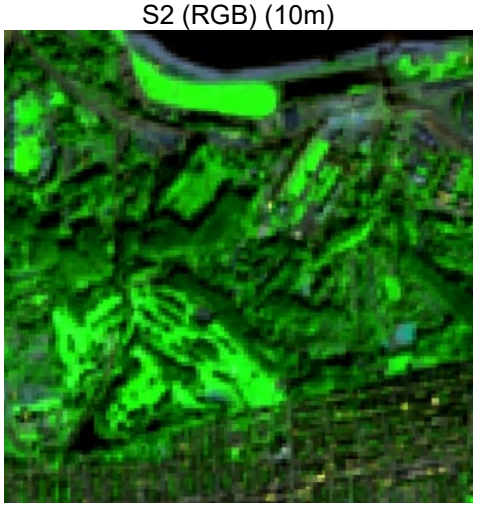

S2 (B5,B8A,B12) (20m)

Area-2

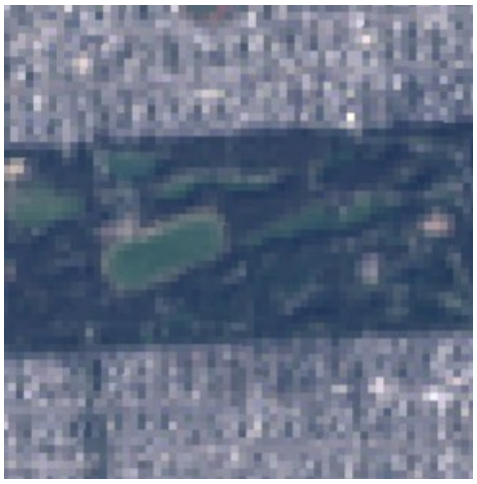

L8 (RGB) (30m)

S2 (RGB) (10m)

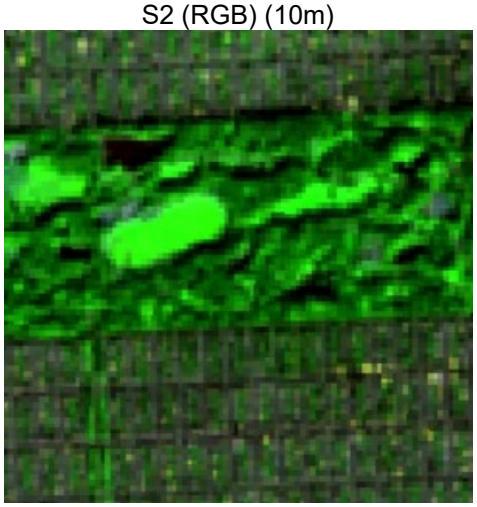

S2 (B5,B8A,B12) (20m)

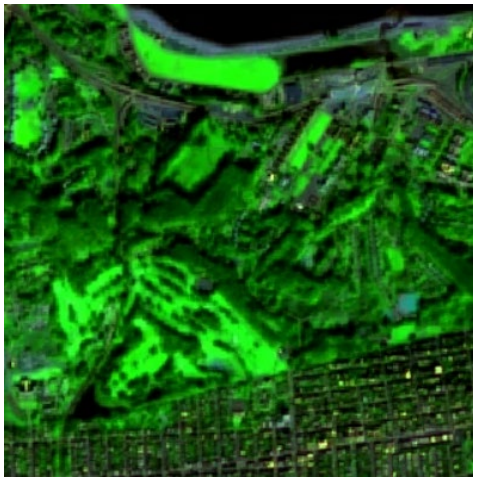

S2 SynPAN (10m)

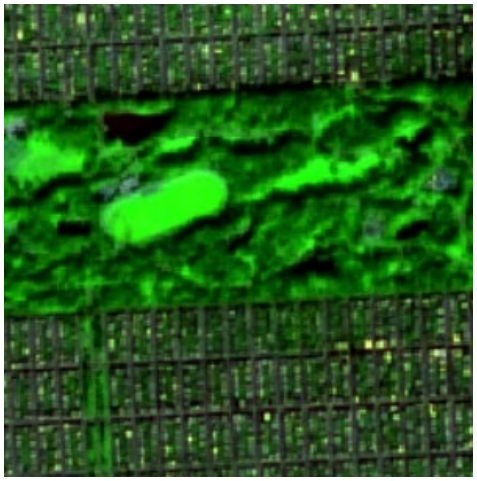

S2 SynPAN (10m)

L8 pan-sharpened with synPAN using GS technique

L8 pan-sharpened with synPAN using GS technique

L8 pan-sharpened with synPAN using SFIM technique

L8 pan-sharpened with synPAN using SFIM technique

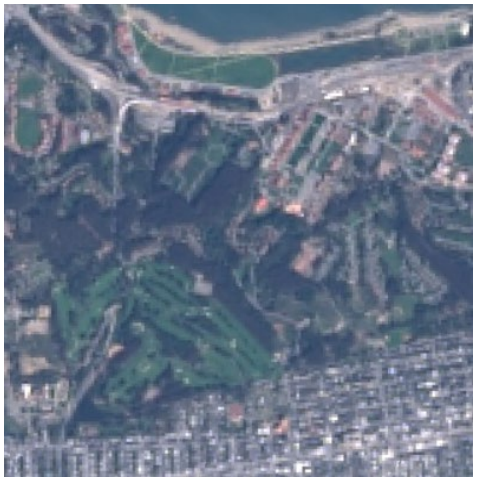

L8 pan-sharpened with synPAN using HPFA technique.

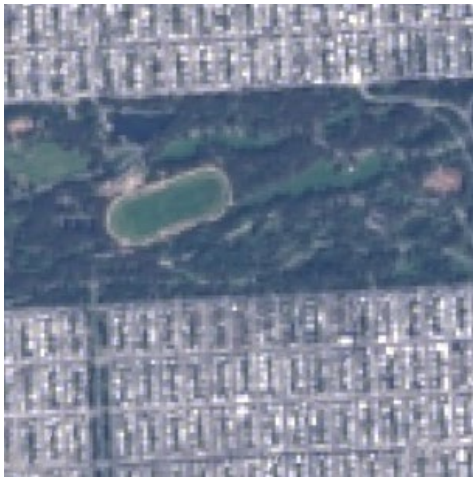

L8 pan-sharpened with synPAN using HPFA technique.

Figure 3. L8 MS images, S2 synPAN images, and pan-sharpened images using three different techniques for area-1 and area-2.

5. Conclusion

L8 image (30m) enhancement was carried out in this research using a synPAN image (10m) generated by averaging the four selected fine-resolution bands from the S2 image, which resulted in a pan-sharpened L8 image (10m). Three different PanS techniques, such as SFIM, GS, and HPFA, were selected for the multi-satellite PanS process, which utilizes satellite images acquired using various sensors with varying spatial resolutions. The techniques' effectiveness was evaluated, and well-known IQAMs such as CC, RMSE, ERGAS, and RASE. Although the qualitative and quantitative comparisons showed slight differences, the GS method emerged as the most effective, while HPFA was the least successful.

Furthermore, the proposed multi-satellite PanS of L8 using synPAN generation from the Senntinel-2 method's applicability was evaluated in two study areas. The proposed approach's feasibility was assessed using statistical tools and visual presentations. These pan-sharpened results find application in land cover classifications, thematic mapping, other visualization purposes, environmental hazard monitoring etc. It is necessary to obtain atmospheric corrected products as it can hinder the accuracy of the results. Another limitation is the turning of hyperparameters in PanS techniques which limit the model's performance. The different SynPAN generation techniques can be explored as a future scope of this study, and an assessment of their performance can be studied by combining them with other PanS techniques to identify the most promising combination. The possibilities of using deep learning techniques for PanS can also be explored and experimented with. This can enhance the land cover land use classification accuracy, object identification, crop identification, and other related applications.

References

[1] C. Pohl and J. L. Van Genderen, "Review article Multisensor image fusion in remote sensing: Concepts, methods and applications," *International Journal of Remote Sensing*, vol. 19, no. 5. pp. 823–854, 1998. doi: 10.1080/014311698215748.

[2] P. Jagalingam and A. V. Hegde, "A Review of Quality Metrics for Fused Image," *Aquat Procedia*, vol. 4, pp. 133–142, 2015, doi: 10.1016/j.aqpro.2015.02.019.

[3] J. and A. V. H. Pushparaj, " Comparison of various pan-sharpening methods using Quickbird-2 and Landsat-8 imagery," *Arabian Journal of Geosciences*, vol. 10, no. 5, pp. 1–17, 2017.

[4] F. DadrasJavan and F. Samadzadegan, "An object-level strategy for pan-sharpening quality assessment of high-resolution satellite imagery," *Advances in Space Research*, vol. 54, no. 11, pp. 2286–2295, Dec. 2014, doi: 10.1016/J.ASR.2014.08.024.

[5] F. Alidoost, M. A. Sharifi, and A. Stein, "Region- and pixel-based image fusion for disaggregation of actual evapotranspiration," *http://dx.doi.org/10.1080/19479832.2015.1055834*, vol. 6, no. 3, pp. 216–231, Jul. 2015, doi: 10.1080/19479832.2015.1055834.

[6] F. Dadrass Javan, F. Samadzadegan, S. Mehravar, A. Toosi, R. Khatami, and A. Stein, "A review of image fusion techniques for pan-sharpening of high-resolution satellite imagery," *ISPRS Journal of Photogrammetry and Remote Sensing*, vol. 171, pp. 101–117, Jan. 2021, doi: 10.1016/J.ISPRSJPRS.2020.11.001.

[7] H. Li, L. Jing, and Y. Tang, "Assessment of Pansharpening Methods Applied to WorldView-2 Imagery Fusion," *Sensors 2017, Vol. 17, Page 89*, vol. 17, no. 1, p. 89, Jan. 2017, doi: 10.3390/S17010089.

[8] M. Hasanlou and M. R. Saradjian, "Quality assessment of pan-sharpening methods in high-resolution satellite images using radiometric and geometric index," *Arabian Journal of Geosciences*, vol. 9, no. 1, pp. 1–10, Jan. 2016, doi: 10.1007/S12517-015-2015-0/FIGURES/8.

[9] C. Pohl and J. L. (John L.) Van Genderen, *Remote sensing image fusion : a practical guide*.

[10] M. Belgiu and A. Stein, "Spatiotemporal image fusion in remote sensing," *Remote Sensing*, vol. 11, no. 7. MDPI AG, 2019. doi: 10.3390/rs11070818.

[11] V. Pandit, V. R. Pandit, and R. J. Bhiwani, "Study of Remote Sensing Image Fusion View project Design and Development of Embedded Systems View project Image Fusion in Remote Sensing Applications: A Review," *Int J Comput Appl*, vol. 120, no. 10, pp. 975–8887, 2015, doi: 10.5120/21263-3846.

[12] G. Kaplan, "Broad-Leaved and Coniferous Forest Classification in Google Earth Engine Using Sentinel Imagery," *Environmental Sciences Proceedings 2021, Vol. 3, Page 64*, vol. 3, no. 1, p. 64, Nov. 2020, doi: 10.3390/IECF2020-07888.

[13] G. Kaur, K. S. Saini, D. Singh, and M. Kaur, "A Comprehensive Study on Computational Pansharpening Techniques for Remote Sensing Images," *Archives of Computational Methods in Engineering*, vol. 28, no. 7, pp. 4961–4978, Dec. 2021, doi: 10.1007/S11831-021-09565-Y/TABLES/3.

[14] H. Ghassemian, "A review of remote sensing image fusion methods," *Information Fusion*, vol. 32. Elsevier B.V., pp. 75–89, Nov. 01, 2016. doi: 10.1016/j.inffus.2016.03.003.

[15] Yuhendra, I. Alimuddin, J. T. S. Sumantyo, and H. Kuze, "Assessment of pan-sharpening methods applied to image fusion of remotely sensed multi-band data," *International Journal of Applied Earth Observation and Geoinformation*, vol. 18, no. 1, pp. 165–175, Aug. 2012, doi: 10.1016/J.JAG.2012.01.013.

[16] J. Duran, A. Buades, B. Coll, C. Sbert, and G. Blanchet, "A survey of pansharpening methods with a new band-decoupled variational model," *ISPRS Journal of Photogrammetry and Remote Sensing*, vol. 125, pp. 78–105, Mar. 2017, doi: 10.1016/J.ISPRSJPRS.2016.12.013.

[17] Q. Du, N. H. Younan, R. King, and V. P. Shah, "On the performance evaluation of pan-sharpening techniques," *IEEE Geoscience and Remote Sensing Letters*, vol. 4, no. 4, pp. 518–522, Oct. 2007, doi: 10.1109/LGRS.2007.896328.

[18] G. Pinheiro and S. Minz, "Image Quality Evaluation of Various Pan-Sharpening Techniques Using Landsat-8 Imagery," pp. 391–403, 2023, doi: 10.1007/978-981-99-1620-7_31.

[19] G. Pinheiro and S. Minz, "Image Quality Assessment Of Spatiotemporal Image Fusion: A Case Study Approach Using Landsat-8 And Sentinel-2," in *43rd Asian Conference on Remote Sensing 2022 (ACRS2022)*, Mongolia: Asian Association on Remote Sensing (AARS), 2022. Accessed: Mar. 16, 2023. [Online].

[20] I. H. Rather and S. Kumar, "Generative adversarial network based synthetic data training model for lightweight convolutional neural networks," *Multimed Tools Appl*, pp. 1–23, May 2023, doi: 10.1007/S11042-023-15747-6/TABLES/3.

[21] N. H. Kaplan and I. Erer, "Ağirliklandirilmiş Dalgacik Dönüşümü ile Pankeskinleştirme," *2016 24th Signal Processing and Communication Application Conference, SIU 2016 - Proceedings*, pp. 781–784, Jun. 2016, doi: 10.1109/SIU.2016.7495856.

[22] H. R. Shahdoosti and N. Javaheri, "Pansharpening of Clustered MS and Pan Images Considering Mixed Pixels," *IEEE Geoscience and Remote Sensing Letters*, vol. 14, no. 6, pp. 826–830, Jun. 2017, doi: 10.1109/LGRS.2017.2682122.

[23] S. D. Jawak and A. J. Luis, "A Comprehensive Evaluation of PAN-Sharpening Algorithms Coupled with Resampling Methods for Image Synthesis of Very High Resolution Remotely Sensed Satellite Data," *Advances in Remote Sensing*, vol. 2013, no. 04, pp. 332–344, Dec. 2013, doi: 10.4236/ARS.2013.24036.

[24] Q. Xu, Y. Zhang, and B. Li, "Recent advances in pansharpening and key problems in applications," *http://dx.doi.org/10.1080/19479832.2014.889227*, vol. 5, no. 3, pp. 175–195, 2014, doi: 10.1080/19479832.2014.889227.

[25] A. Raj and S. Minz, "A Scalable Unsupervised Classification Method Using Rough Set for Remote Sensing Imagery," *International Journal of Software Science and Computational Intelligence*, vol. 13, no. 2, pp. 65–88, Apr. 2021, doi: 10.4018/IJSSCI.2021040104:

[26] G. Kaplan and U. Avdan, "Sentinel-2 Pan Sharpening—Comparative Analysis," *Proceedings 2018, Vol. 2, Page 345*, vol. 2, no. 7, p. 345, Mar. 2018, doi: 10.3390/ECRS-2-05158.

[27] Q. Wang, W. Shi, Z. Li, and P. M. Atkinson, "Fusion of Sentinel-2 images," *Remote Sens Environ*, vol. 187, pp. 241–252, Dec. 2016, doi: 10.1016/J.RSE.2016.10.030.

[28] M. Selva, B. Aiazzi, F. Butera, L. Chiarantini, and S. Baronti, "Hyper-sharpening: A first approach on SIM-GA data," *IEEE J Sel Top Appl Earth Obs Remote Sens*, vol. 8, no. 6, pp. 3008–3024, Jun. 2015, doi: 10.1109/JSTARS.2015.2440092.

[29] M. Gašparović and T. Jogun, "The effect of fusing Sentinel-2 bands on land-cover classification," *https://doi.org/10.1080/01431161.2017.1392640*, vol. 39, no. 3, pp. 822–841, Feb. 2017, doi: 10.1080/01431161.2017.1392640.

[30] N. Gorelick, M. Hancher, M. Dixon, S. Ilyushchenko, D. Thau, and R. Moore, "Google Earth Engine: Planetary-scale geospatial analysis for everyone," *Remote Sens Environ*, vol. 202, pp. 18–27, Dec. 2017, doi: 10.1016/J.RSE.2017.06.031.

[31] L. Kumar and O. Mutanga, "Google Earth Engine Applications Since Inception: Usage, Trends, and Potential," *Remote Sensing 2018, Vol. 10, Page 1509*, vol. 10, no. 10, p. 1509, Sep. 2018, doi: 10.3390/RS10101509.

[32] H. Tamiminia, B. Salehi, M. Mahdianpari, L. Quackenbush, S. Adeli, and B. Brisco, "Google Earth Engine for geo-big data applications: A meta-analysis and systematic review," *ISPRS Journal of Photogrammetry and Remote Sensing*, vol. 164, pp. 152–170, Jun. 2020, doi: 10.1016/J.ISPRSJPRS.2020.04.001.

[33] G. Pinheiro, A. Raj, · Sonajharia Minz, T. Choudhury, and J.-S. Um, "Inundation extend mapping for multi-temporal SAR using automatic thresholding and change detection: a case study on Kosi river of India," *Spatial Information Research*, vol. 1, p. 3, doi: 10.1007/s41324-023-00555-9.

[34] A. Capolupo and E. Tarantino, "Landsat 9 Satellite Images Potentiality in Extracting Land Cover Classes in GEE Environment Using an Index-Based Approach: The Case Study of Savona City," *Lecture Notes in Computer Science (including subseries Lecture Notes in Artificial Intelligence and Lecture Notes in Bioinformatics)*, vol. 14107 LNCS, pp. 251–265, 2023, doi: 10.1007/978-3-031-37114-1_17/COVER.

[35] L. Lin *et al.*, "Monitoring Land Cover Change on a Rapidly Urbanizing Island Using Google Earth Engine," *Applied Sciences 2020, Vol. 10, Page 7336*, vol. 10, no. 20, p. 7336, Oct. 2020, doi: 10.3390/APP10207336.

[36] L. Korhonen, Hadi, P. Packalen, and M. Rautiainen, "Comparison of Sentinel-2 and Landsat 8 in the estimation of boreal forest canopy cover and leaf area index," *Remote Sens Environ*, vol. 195, pp. 259–274, Jun. 2017, doi: 10.1016/J.RSE.2017.03.021.

[37] U. G. , P. S. P. and D. W. Holcomb. Gangkofner, "Optimizing the high-pass filter addition technique for image fusion," *Photogrammetric Engineering & Remote Sensing* , vol. 73, no. 9, pp. 1107–1118, 2007.

[38] G. Sarp, "Spectral and spatial quality analysis of pan-sharpening algorithms: A case study in Istanbul," *http://dx.doi.org/10.5721/EuJRS20144702*, vol. 47, no. 1, pp. 19–28, Feb. 2017, doi: 10.5721/EUJRS20144702.

[39] J. G. Liu, "Smoothing Filter-based Intensity Modulation: A spectral preserve image fusion technique for improving spatial details," *http://dx.doi.org/10.1080/014311600750037499*, vol. 21, no. 18, pp. 3461–3472, 2010, doi: 10.1080/014311600750037499.

[40] L. Alparone, B. Aiazzi, S. Baronti, A. Garzelli, F. Nencini, and M. Selva, "Multispectral and panchromatic data fusion assessment without reference," *Photogramm Eng Remote Sensing*, vol. 74, no. 2, pp. 193–200, 2008, doi: 10.14358/PERS.74.2.193.

[41] S. Panchal and R. Thakker, "Signal & Image Processing," *An International Journal (SIPIJ)*, vol. 6, no. 5, 2015, doi: 10.5121/sipij.2015.6503.